

Personal Sound Zones and Shielded Localized Communication through Active Acoustic Control

Neil Jerome A. Egarguin¹, Daniel Onofrei²

¹Institute of Mathematical Sciences, University of the Philippines Los Baños
College, Laguna, Philippines

²Department of Mathematics, University of Houston, Houston, TX, USA

Abstract

In this paper, we present a time domain extension of our strategy on manipulating radiated scalar Helmholtz fields and discuss two important applied scenarios, namely (1) creating personal sound zones inside a bounded domain and (2) shielded localized communication. Our strategy is based on the authors' previous works establishing the possibility and stability of controlling acoustic fields using an array of almost non-radiating coupling sources and presents a detailed Fourier synthesis approach towards a time-domain effect. We require that the array of acoustic sources creates the desired fields on the control regions while maintaining a zero field beyond a larger circumscribed sphere. This paper recalls the main theoretical results then presents the underlying Fourier synthesis paradigm and show, through relevant simulations, the performance of our strategy.

1 Introduction

The research presented in this paper aims at investigating novel modalities for the characterization of feasible acoustic sources (i.e., position and feed inputs for active radiators) towards the active manipulation of their radiated fields in prescribed exterior regions and/or desired far field directions, with applications in localized communication and the realization of personal sound zones. There exists a vast body of literature on computational and analytical methods for acoustic scattering and radiation, such as the major monographs [82, 69].

Regarding the problem of active manipulation of acoustic fields, two of the earliest works concern the active control of sound, i.e., [60] (feed-forward control of sound) and [74] (feedback control of sound). The general problem of active control of scalar Helmholtz fields is discussed in [85, 47, 63, 66, 65, 64, 81, 41, 80, 73, 39, 4, 52, 71, 94, 92, 63, 66, 48, 49, 70, 100, 99]. Energy localization results for Helmholtz scalar fields obtained via Runge approximations are discussed for the interior problem in [83] and for the scattering problem in [5, 45, 46], (see also recent thesis [8] and the study in [9] for localized wave functions in a waveguide).

The applications of acoustic field control include active noise cancellation ([72, 44, 17, 58, 68]), sound synthesis and reproduction ([4, 56, 75, 99, 91, 59, 42, 43]), and active control of acoustic scattered fields with application to cloaking and shielding ([54, 19, 12, 94, 92, 93, 62, 38, 67]). A more comprehensive discussion and analysis of some of the methods employed in these applications is also given in [16] for scattered field control, in [55, 57, 15, 13] for direct problems in ocean and layered media and in [40, 2, 95, 20, 21, 1], for general sound field control.

Boundary integral operators were used in [76, 77] to produce a stable unified control strategy in the case of a single active surface source proving the active control of scalar radiated fields in prescribed exterior region of space. These theoretical results were later extended by the authors' group to consider active scalar sources in ocean environments, free space or layered media, and applied to relevant 2D and 3D numerical studies in [53, 78, 34, 37, 35, 86, 36]. In [11], the proposed active manipulation methods were extended and applied to the case where impenetrable obstacles were assumed present as well.

Practical implementation of such strategies may require accurate field measurements, or the use of non-traditional sources. In this regard and in the context of scattered field active control, the authors in [63, 50, 52] proposed methods which are only based on measurements of the total field around the sources, while in a more general context, in [96, 97] the authors proposed methods to overcome the difficult task of using monopolar sources in the control schemes proposed in the literature. Nanometer size sources are recently being proposed in the literature based on strong variations of thermal effects in special materials nano-tubes ([14, 90, 51]).

The problem of field synthesis requires the construction of feed inputs on the active sources for the approximation of a given far field pattern [7, 3] ("the far field synthesis") (see also the monograph [22] where general radiation theory and source synthesis techniques are discussed). The problem of field focusing is mainly formulated in terms of power maximization in the far field (with eventual nulls in prescribed far field directions) and analyzed through an associated eigenvalue problem stemming from first order optimality conditions imposed to an associated augmented Lagrangian (see the monograph [7]).

The problem of using active sources for creating highly localized patterns in prescribed regions of space with specified fields in given far field directions in general media is of potential high interest for many possible applications (see [6], [5], [45] and [46] for scattering energy localization results with applications to inverse obstacle problems as well as [8] and [9]).

Regarding the problem of time domain active field manipulation, we studied in [34] the scalar case and by using superposition we produced simulations suggesting the possibility of using our scalar control theory for the characterization of causal sources so that their radiated fields approximate a given time domain signal in a near field region while maintaining a very small field in another exterior region.

In what follows, we will use our theoretical results on the active manipulation of fixed frequency Helmholtz fields reported in [77, 53, 78, 34, 37, 35, 86, 36] to build a detailed Fourier synthesis approach towards time domain active control as applied to two application scenarios:

- the realization of personal sound zones inside a bounded domain; and
- shielded localized communications, i.e., design of an array of sources with a personal listening area and a fast decaying acoustic field.

Section 2 presents the problem in mathematical parlance, while Section 3 and Section 4 respectively discuss the mathematical and numerical frameworks of the proposed solution scheme. Section 5 shows the implementation of the solution scheme through several numerical simulations of the scenarios mentioned above. The section includes a detailed formulation of the time-domain synthesis via Fourier analysis. The paper ends with some concluding remarks in Section 6.

2 Statement of the Problem

Mathematically, the general question is to find acoustic pressure p_j or normal velocity v_j , $j = \overline{1, n}$ on the surface of n acoustic sources D_j , $j = \overline{1, n}$, so that the solution u of the Helmholtz problem in the exterior of the sources given by

$$\begin{cases} \Delta u + k^2 u = 0 \text{ in } R \setminus \left(\bigcup_{j=1}^n \overline{D}_j \right), \\ \nabla u \cdot \mathbf{n}_j = v_j, \text{ (or } u = p_j \text{) on } \partial D_j, j = \overline{1, n} \\ \text{suitable condition on } \partial R \end{cases} \quad (1)$$

approximates some predetermined fields f_p on m control regions $R_p \Subset R \setminus \left(\bigcup_{j=1}^n \overline{D}_j \right)$, $p = \overline{1, m}$

interior to R , where the region R could be a bounded domain encompassing the sources and the control regions or the whole space \mathbb{R}^3 in which case the boundary condition in (1) above becomes the classical Sommerfeld outgoing condition at infinity.

In our first application we consider the creation of personal sound zones in a car cabin, i.e., where R is the region of the car interior. Figure 1 shows a typical car cabin where we wish to generate predetermined sound profiles in the vicinity of each passenger, i.e., the control regions inside the blue spheres using speakers (sound sources) represented by red dots located in the headrest of each seat. This will allow each passenger to enjoy their acoustic preference with minimal to no interference with each other. One of the main difficulty with this application, besides the active control of the sources to create personalized sound experiences on each of the control regions, is the effect of the boundary of R . In the case of a car cabin, the boundary is composed of different materials such as glass, hard plastics, metal, leather, etc. The different reaction of these materials to sound makes the boundary condition in (1) difficult to model. Moreover, the boundary condition on ∂R may play a crucial role in the propagation of acoustic waves as it determines the reverberations of sound created by the sources back into the cabin.

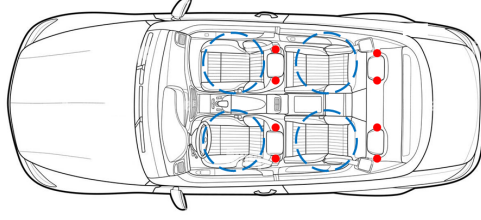


Figure 1: Personal Sound Zones in a Car Cabin: In this application, we create sound profiles in the control regions inside the blue spheres using the speakers drawn as red dots

The second application we consider is that of shielded localized communication, i.e., where R denotes the whole space. In this case, the goal is to realize a free space communication zone shielded from the exterior by maintaining a very small field outside a given circumscribed sphere as sketched in Figure 2 where, not appearing in the sketch, the fields are required to decay to very small levels beyond a radius of 1.5 meters. The main difficulty in this application is the fact that we want a good control in the designated listening region with a very fast decay of the fields while maintaining a rather low uniform energy distribution in the region between the sources and the control areas for an overall smooth sound scene.

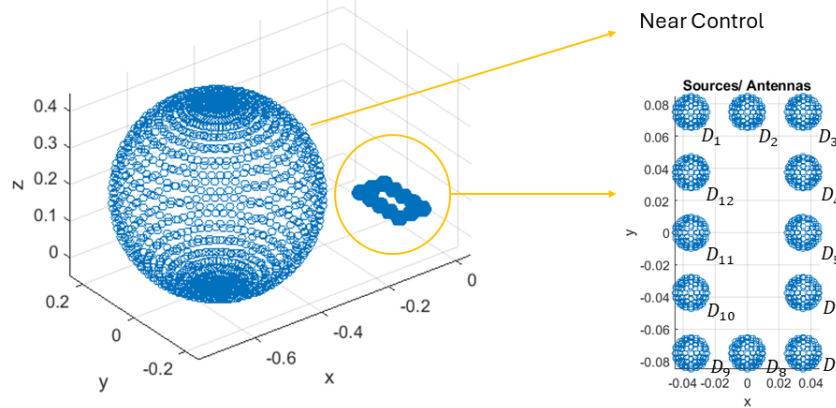


Figure 2: Shielded Localized Communication: In this application, we create a desired sound profile in the near control using the sources while requiring the acoustic field to decay fast

To address these issues, we propose a scheme that takes advantage of our previous works [77, 78, 34, 37] and employs a Fourier synthesis scheme towards a time-domain control effect. The central idea of our solution requires field pattern matching in the control regions with fast enough decay of the generated acoustic field so that either the reverberations from the boundary ∂R are insignificant insofar as creating unwanted interference in the sound produced in each control region for the car cabin scenario, or that very little perturbation outside the listening area in the shielded communication application. Details of this scheme are discussed in the following section.

3 Mathematical Framework

In this section, we discuss the mathematical framework of our proposed solution to the acoustic control problem in enclosed environments described in the previous section. The foundation of our proposed solutions rests on the possibility of creating an almost non-radiating acoustic field in the interior of the region R using the sources D_j , $j = \overline{1, n}$ with the requirement that this generated field approximates the prescribed fields f_p on the interior control regions R_p . The framework described below were established in previous works [77, 78, 34, 37].

Let $\{R_1, R_2, \dots, R_m\}$ be a collection of m mutually disjoint smooth domains inside $R \subseteq \mathbb{R}^3$ where R_m is the exterior of some large enough null sphere $R \setminus B_r(\mathbf{0})$ for some prescribed value of $r > 0$. These domains will be referred to as the control regions. The problem is to generate a prescribed acoustic field in R_p , $p = \overline{1, m}$ using a collection of active sources $\{D_1, D_2, \dots, D_n\}$ modeled as mutually disjoint compact regions in R with Lipschitz continuous boundaries. It is assumed that the sources and control regions are well-separated from each other. Formally, the problem is to find some appropriate boundary input on these sources, either a normal velocity $v_j \in C(\partial D_j)$ or an acoustic pressure $p_j \in C(\partial D_j)$, $j = \overline{1, n}$, such that for any desired field $f = (f_1, f_2, \dots, f_m)$ on the control regions, the solution u of the following problem

$$\begin{cases} \Delta u + k^2 u = 0 \text{ in } \mathbb{R}^3 \setminus \left(\bigcup_{j=1}^n \overline{D}_j \right), \\ \nabla u \cdot \mathbf{n}_j = v_j, \text{ (or } u = p_j \text{) on } \partial D_j, \quad j = \overline{1, n} \\ \langle \hat{x}, \nabla u(x) \rangle - iku(x) = o\left(\frac{1}{|x|}\right), \text{ as } |x| \rightarrow \infty \text{ uniformly for all } \hat{x}, \end{cases} \quad (2)$$

satisfies the control constraint

$$\|u - f_p\|_{C^2(R_p)} \leq \mu \text{ for } l = \overline{1, m} \quad (3)$$

where μ is some small positive parameter, $C^2(M)$ denotes the space of functions defined on M with continuous partial derivatives up to the second order, and \mathbf{n}_j is the outward unit normal to ∂D_j and $\hat{x} = \frac{x}{|x|}$ denotes the unit vector along the direction x . As a convention, the $e^{-i\omega t}$ ($w = kc$) of the fields is implicitly assumed and omitted for the simplicity of analysis in the fixed frequency case.

Following the formulation in [77], the solution to (2) - (3) is assumed to be a layer potential. Provided k is not a resonance (see [18] and [77], [78]), the boundary input (normal velocity v_j or pressure p_j) on each source D_j can be characterized by a density function w_j such that

$$v_j(x) = \frac{-i}{\rho ck} \frac{\partial}{\partial \mathbf{n}_1} \int_{\partial D'_j} w_j(y) \phi_\omega(x, y) dS \text{ and} \quad (4)$$

$$p_j(x) = \int_{\partial D'_j} w_j(y) \phi_\omega(x, y) dS, \quad (5)$$

where D'_j is a fictitious source that is compactly embedded in D_j and ϕ_ω is the fundamental solution of the Helmholtz problem at fixed frequency $\omega = kc$ in free space. Although the expressions in (4) and (5) make use of the single layer potential operator, it was shown in [78] (see also [34]) that appropriate boundary inputs can be obtained by using the single layer potential representation or more generally, a representation given by a linear combination of single and double layer potentials which can actually remove the condition that k is not a resonance. Moreover, it was noted in the aforementioned works that the control of the acoustic fields in the entire volume of each control region R_p can be ensured by controlling the acoustic field on the surface of a slightly larger control region W_p that compactly embeds R_p , by appealing to the uniqueness and regularity properties of the solutions of the interior problem (2).

In [37], the solution of the forward interior problem (2) was defined through the operator

$$\mathcal{D} : \prod_{j=1}^n L^2(\partial D'_j) \rightarrow \prod_{p=1}^m L^2(\partial W_p)$$

that takes as input the density function $w = (w_1, w_2, \dots, w_n)$, whose components are defined on the surface of the fictitious sources, that characterize the boundary input via (4) or (5) and produces the output $\mathcal{D}w$ representing the generated field on the surface of the slightly larger control regions (W_1, W_2, \dots, W_m) . It should be noted that the operator \mathcal{D} takes into account the first-order coupling among the sources. The two main results of [37] pertinent to this study are as follows.

Theorem 3.1. *[[37], Theorem 2.2] The compact operator \mathcal{D} has a dense range.*

Theorem 3.2. *[[37], Proposition 3.1] The solution scheme proposed in [37] is stable with respect to perturbations of the prescribed field to be synthesized.*

Theorem 3.1 guarantees that for any Helmholtz field $f = (f_1, f_2, \dots, f_m) \in \prod_{p=1}^m L^2(\partial W_p)$,

there exists an infinity of solutions $w = (w_1, w_2, \dots, w_n) \in \prod_{j=1}^n L^2(\partial D'_j)$ such that

$$\mathcal{D}w \approx f \tag{6}$$

for any given accuracy threshold. Meanwhile, Theorem 3.2 states that the solution of the perturbed equation

$$\mathcal{D}w \approx f + \epsilon s \tag{7}$$

where s is a unit noise vector and $0 < \epsilon \ll 1$, is close to the solution of the unperturbed equation (6).

We take advantage of these results to address the acoustic control problem (1) in the case of enclosed environments with complex boundaries. For instance, in the problem of creating personalized sound zones in car cabins, we consider the abstracted problem geometry shown

in Figure 3. The control regions were represented by the blue dots while the boundary of the cabin is illustrated as the solid rectangle. Instead of modeling the boundary condition, we introduce a fictitious null sphere, shown as the orange circle, that encloses the control region but is separated from the boundary. We shall require our acoustic sources to not only approximate the prescribed fields on the control regions, but also to create a near zero acoustic field on the surface of the null sphere. The uniqueness and stability of the exterior problem dictates that the acoustic field beyond the null sphere will be small enough so that the reverberations caused by the reflection of the acoustic fields on the boundary will not have a large impact on the established acoustic profiles on the control regions.

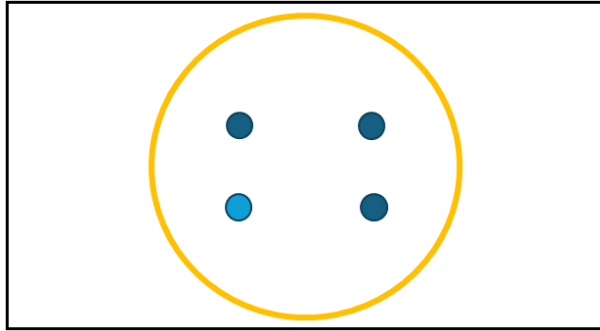


Figure 3: An abstraction of the car cabin environment, the solid rectangle represents the enclosure of the cabin while the dots represent the control regions and the orange sphere represents the null sphere

This novel approach removes the necessity of modeling the complex boundary condition for (1) which may then require tedious calculations and analysis of the appropriate Green’s function. In the following sections, we shall present some numerical simulations that illustrates this control strategy.

4 Numerical Framework

In this section, we discuss the framework for the numerical solution of (2)-(3) adapted to the geometry suggested in the previous section where a fictitious null sphere that contains the control regions and is well-separated from the environment’s boundary was introduced. The framework was originally broached in the works [77, 78, 34, 37].

As in[37], we shall use local basis functions to reduce the operatorial equation $\mathcal{D}w = f$ to a linear system $Ac = b$. A detailed discussion of local basis functions applied to finite element methods in acoustics and electromagnetics can be found in [84]. We discretize the surface of each fictitious source D'_j into a set $\{T_j^1, T_j^2, \dots, T_j^N\}$ of triangular elements such that each vertex of the triangle lies on the surface of the fictitious source. Then for each vertex v_i of q^{th} triangle T_j^q , we associate a linear interpolating function N_i such that $N_i(v_i) = 1$ and zero on the other two vertices. Thus, for every $x \in T_j^q$, the unknown density function w_j can

be expressed by the linear interpolant

$$w_{j,q}(x) = \sum_{i=1}^3 c_i N_i(x), \quad (8)$$

where the coefficient c_i is the value of w_j on vertex v_i . At this point, the continuous problem of finding the density function $w = (w_1, w_2, \dots, w_n) \in \prod_{j=1}^n L^2(\partial D'_j)$ is reduced to solving for the coefficients $c_i \in \mathbb{C}$.

To fully discretize the equation $\mathcal{D}w = f$, we shall use collocation test points from a dense mesh of points from each W_p . If there is a total of M discretization points on the control regions and a total of N points on the surface of the fictitious sources then the matrices A , c and b in the discrete approximation of the operatorial equation are of dimensions $M \times N$, $N \times 1$ and $M \times 1$, respectively. Each entry of the matrix A is an integral approximated using the standard seven-point Gaussian quadrature rule. Then the unknown vector c of basis coefficients is computed as the Tikhonov solution

$$c = (\alpha I + A^* A)^{-1} A^* b \quad (9)$$

with the regularization parameter α chosen using the Morozov discrepancy principle. See [78] for a detailed discussion of the Tikhonov regularization routine using the Morozov discrepancy principle.

The approximate solution for the operatorial equation $\mathcal{D}w \approx f$ obtained by implementing the mathematical framework described in the previous section through the numerical scheme discussed above appears to be stable with respect to process errors. That is, for a solution w of $\mathcal{D}w \approx f$, a unit noise vector s and small enough noise level ϵ with $0 < \epsilon \ll 1$,

$$\mathcal{D}(w + \epsilon s) \approx f \quad (10)$$

still holds. This can be observed in the simulations in [86], where a detailed feasibility study was conducted for sources in free space and in shallow water environments. These suggest that there is a level of error or noise in the manufacturing of the sources that will not significantly ruin the control effect.

In the next section, we present several simulations illustrating the scheme discussed above. A total of 234 basis functions were used on each spherical fictitious source modeling the actual physical source, while the control regions are discretized depending on the target application. As a computational stability check, these evaluation points are chosen to be the midpoint between consecutive points in the original mesh of collocation points used together with the local basis discretization to obtain the solution (9) to the associated linear system. We also calculate the pointwise relative error $\frac{|f_l(x) - u_l(x)|}{|f_l(x)|}$ and take note of its supremum. Whenever W_p is the null sphere, we observe the supremum magnitude of the generated field in W_p .

5 Numerical Simulations

In this section, we present the two applications of this work: personal sound zones inside a bounded region and shielded localized communication. The sections present several numerical simulations associated with each of these two applications and illustrate the quality of our controls.

5.1 Personal Sound Zones in Car Cabins

For the case of creating personal sound zones within a car cabin, we shall present two simulations. In the first, we present a static case where we create four planewaves of different frequencies while in the second, we present a time-domain simulation using Fourier synthesis. In both cases, we use a total of eight sources with two sources near each control region. They are all spheres of radius 5 cm positioned relative to their proximal control region in the same way as Figure 1. The control regions are also spheres of radius 10 cm positioned inside the car cabin as shown in Figure 3. These control regions, including the null sphere, is discretized into 1250 collocation points.

5.1.1 Multi-frequency Simulation

In this test, we prescribe planewaves $f_p(\mathbf{x}) = e^{i\mathbf{x} \cdot (k_p \hat{\mathbf{d}}_p)}$, $p = \overline{1,4}$ of different propagation directions and frequencies on each control region. The directions of propagation are $\mathbf{d}_1 = \langle 0, 1, 0 \rangle$, $\mathbf{d}_2 = \langle 1, 0, 0 \rangle$, $\mathbf{d}_3 = \langle 0, 0, 1 \rangle$, and $\mathbf{d}_4 = \langle 0, \frac{\sqrt{2}}{2}, \frac{\sqrt{2}}{2} \rangle$ while the wave numbers are $k_1 = 10, k_2 = 15, k_3 = 20, k_4 = 25$, corresponding to frequencies 545.90 Hz, 818.85 Hz, 1.09 KHz, and 1.36 KHz, respectively.

Figure 4 shows a very good approximation of the desired patterns in each of the control regions. In fact, the pointwise relative errors are kept below 5.58 % as seen in Figure 5.

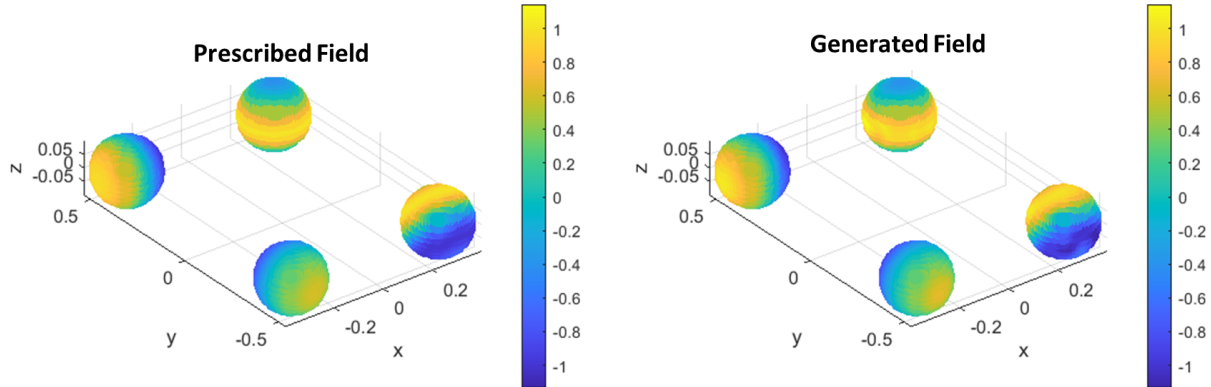


Figure 4: A visual comparison of the real part of the prescribed and generated fields

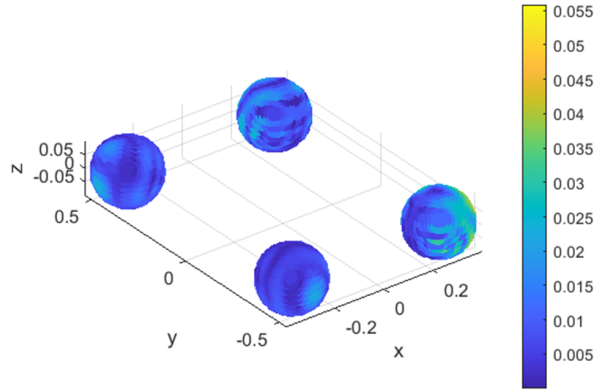


Figure 5: Plot of the pointwise relative error

Likewise, good results were obtained on the surface of the null sphere. Figure 6 shows that the generated field has supremum norm of around 3.88×10^{-2} and has values of order 10^{-3} in most of the sphere's surface.

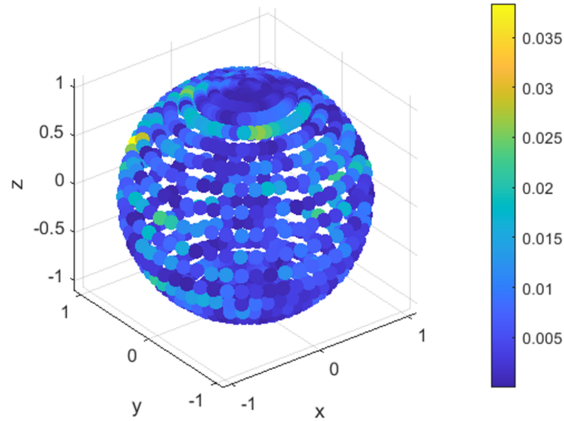


Figure 6: Plot of the pointwise magnitude of the generated field in the surface of the null sphere

The computed densities on the surface of the fictitious sources D'_j obtained from the numerical scheme and the resulting normal velocities on each physical source D_j are shown in Figure 7 and Figure 8, respectively. These show the existence of complex patterns with oscillations that may require non-standard approaches in the physical synthesis of the sources.

This simulation illustrates the possibility of simultaneously creating different sound profiles, even with varying frequency and direction of propagation, on the control regions that will decay fast in space. This fast decay ensures that the reverberations from the boundary

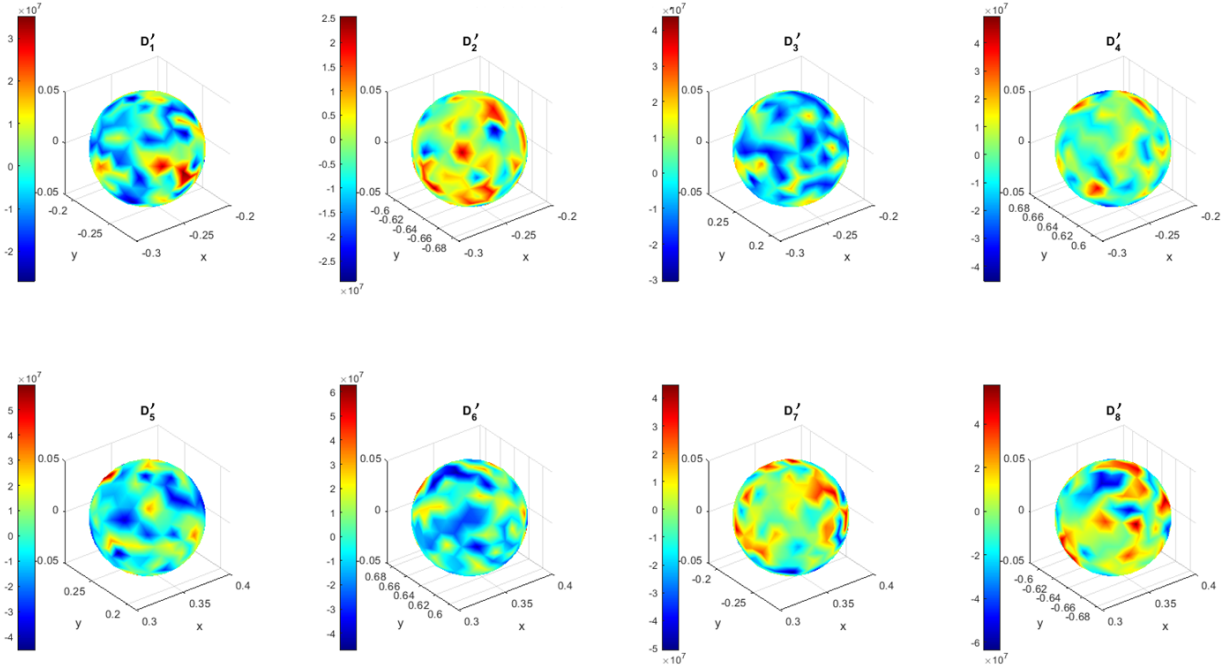


Figure 7: Real part of the computed density on the fictitious sources

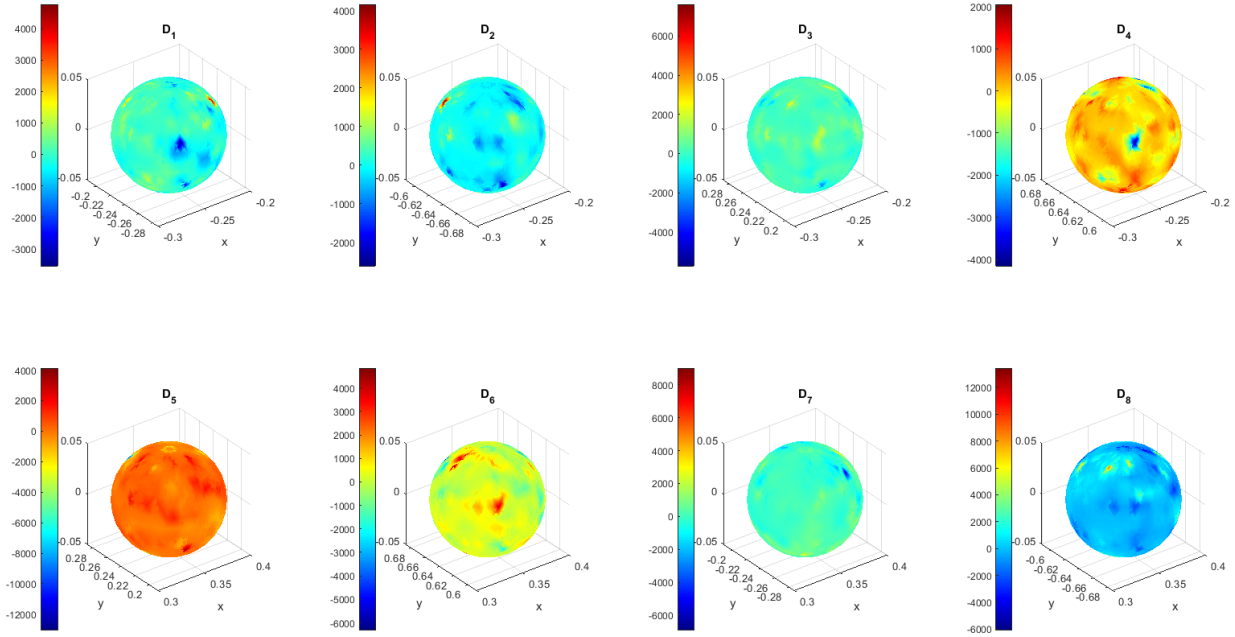


Figure 8: Real part of the corresponding normal velocity on the physical sources

of the cabin will not significantly affect the quality of the synthesized field.

5.1.2 Time-domain Framework

In this subsection, we present the Fourier synthesis scheme for a time-domain extension of the control problem discussed above, a scheme that will again be employed further in the paper for the second time-domain simulation discussing shielded localized sound (presented later in Section 5.2). Assume that the desired target to be approximated is given in the time domain by

$$z(x, t) = \sum_{j=1}^N e^{-i\omega_j t} f_j(x) \text{ in } \Omega, \quad (11)$$

where $\Omega = \left(\bigcup_{s=1}^{m-1} R_s \right) \bigcup \partial R_m$ is the control region and the f_j 's are the solutions of the Helmholtz equation in the neighborhoods of $R_s, s = \overline{1, m}$ with frequency ω_j for $j = \overline{1, N}$. We will approximate the field in (11) by building time harmonic approximations for each individual frequency and then employing superposition through Fourier synthesis.

Let $\bigcup_{j=1}^n D'_j = D'_a \subset \bigcup_{j=1}^n D_j = D_a$ and $\omega = \omega_0$ be a fixed frequency. We want to first find the time domain source input $q(y, t)$ which will produce the desired radiation to be approximated $e^{-i\omega_0 t} f(x)$ where f solves the Helmholtz equation in a neighborhood of Ω . Let

$$q(y, t) = e^{-i\omega_0 t} w(y) (H(t) - H(t - T)) \quad (12)$$

where $H(t) = \begin{cases} 1, & t > 0 \\ 0, & t < 0 \end{cases}$ is the Heaviside step function and w is a source density distributed

on $\partial D'_a = \bigcup_{j=1}^n \partial D'_j$ and $T > 0$ is the large enough final time to be chosen later. Then by Fourier transform, we have that the acoustic field corresponding to this time domain source is given by

$$v(x, t) = \frac{1}{2\pi} \int_{-\infty}^{+\infty} \int_{\partial D'_a} \phi_\omega(x, y) \hat{q}(y, \omega) e^{-i\omega t} dS_y d\omega \quad (13)$$

where

$$\hat{q}(y, \omega) = \int_{-\infty}^{+\infty} q(y, t) e^{i\omega t} dt = \int_0^T q(y, t) e^{i\omega t} dt \quad (14)$$

based on (12). Using (12) in (14) yields

$$\begin{aligned} \hat{q}(y, \omega) &= \int_{-\infty}^{+\infty} e^{-i\omega_0 t} w(y) e^{i\omega t} (H(t) - H(t - T)) \\ &= w(y) \left[\int_{-\infty}^{+\infty} e^{i(\omega - \omega_0)t} H(t) dt - \int_{-\infty}^{+\infty} e^{i(\omega - \omega_0)t} H(t - T) dt \right] \\ &= w(y) (\hat{H}(\omega - \omega_0) - e^{i(\omega - \omega_0)T} \hat{H}(\omega - \omega_0)), \end{aligned} \quad (15)$$

where we applied the change of variable $t = \tilde{t} + T$ in the last integral above and where \hat{H} denotes the Fourier transform of H .

Using (15) in (13), we obtain

$$v(x, t) = \frac{1}{2\pi} \int_{-\infty}^{+\infty} \int_{\partial D'_a} \phi_\omega(x, y) w(y) \hat{H}(\omega - \omega_0) \left((1 - e^{i(\omega - \omega_0)T}) e^{-i\omega t} \right) dS_y d\omega. \quad (16)$$

Note that

$$\begin{aligned} \phi_\omega(x, y) &= \frac{e^{ik|x-y|}}{4\pi|x-y|} = \frac{e^{i\omega \frac{|x-y|}{c}}}{4\pi|x-y|} = \frac{e^{i(\omega - \omega_0) \frac{|x-y|}{c}}}{4\pi|x-y|} \cdot e^{i\omega_0 \frac{|x-y|}{c}} \\ &= \phi_{\omega_0}(x, y) \cdot e^{i(\omega - \omega_0) \frac{|x-y|}{c}}, \end{aligned} \quad (17)$$

where c is the speed of sound in the medium. Using (17) in (16), we get

$$\begin{aligned} v(x, t) &= \frac{1}{2\pi} \int_{-\infty}^{+\infty} \int_{\partial D'_a} \phi_{\omega_0}(x, y) w(y) e^{i(\omega - \omega_0) \frac{|x-y|}{c}} \hat{H}(\omega - \omega_0) (1 - e^{i(\omega - \omega_0)T}) e^{-i\omega t} dS_y d\omega \\ &= \frac{1}{2\pi} \int_{\partial D'_a} \phi_{\omega_0}(x, y) w(y) \int_{-\infty}^{+\infty} e^{i(\omega - \omega_0) \frac{|x-y|}{c}} \hat{H}(\omega - \omega_0) (1 - e^{i(\omega - \omega_0)T}) e^{-i\omega t} d\omega dS_y. \end{aligned} \quad (18)$$

Note that

$$\begin{aligned} &\int_{-\infty}^{+\infty} e^{i(\omega - \omega_0) \frac{|x-y|}{c}} \hat{H}(\omega - \omega_0) (1 - e^{i(\omega - \omega_0)T}) e^{-i\omega t} d\omega \\ &= e^{-i\omega_0 t} \int_{-\infty}^{+\infty} e^{i\tilde{\omega} \frac{|x-y|}{c}} \hat{H}(\tilde{\omega}) (1 - e^{i\tilde{\omega}T}) e^{-i\tilde{\omega}t} d\tilde{\omega} \\ &= e^{-i\omega_0 t} \cdot 2\pi \cdot \left[H\left(t - \frac{|x-y|}{c}\right) - H\left(t - T - \frac{|x-y|}{c}\right) \right] \end{aligned} \quad (19)$$

where we used the change of variable $\omega - \omega_0 = \tilde{\omega}$. Using (19) in (18) gives

$$v(x, t) = e^{-i\omega_0 t} \int_{\partial D'_a} \left[H\left(t - \frac{|x-y|}{c}\right) - H\left(t - T - \frac{|x-y|}{c}\right) \right] \phi_{\omega_0}(x, y) w(y) dS_y. \quad (20)$$

Thus, if the density w is such that

$$\int_{\partial D'_a} \phi_{\omega_0}(x, y) w(y) dS_y \approx f(x) \text{ in } \Omega. \quad (21)$$

From (21), we will have that for given $x \in \Omega$

$$v(x, t) \approx e^{-i\omega_0 t} f(x), \quad (22)$$

in the time interval prescribed by

$$\max_{y \in \partial D_a} \frac{|x - y|}{c} < t < \min_{y \in \partial D_a} \frac{|x - y|}{c} + T. \quad (23)$$

Thus, from (22) and (23) we obtain that

$$v(x, t) \approx e^{-i\omega_0 t} f(x) \text{ holds for all } x \in \Omega,$$

in the following time interval:

$$t_1 = \max_{x \in \Omega} \max_{y \in \partial D_a} \frac{|x - y|}{c} < t < \min_{x \in \Omega} \min_{y \in \partial D_a} \frac{|x - y|}{c} + T = t_2. \quad (24)$$

Note that (24) imposes a restriction on T and the geometry of our problem as, for example, (24) necessarily implies that

$$t_1 = \max_{x \in \Omega} \max_{y \in \partial D_a} \frac{|x - y|}{c} < \min_{x \in \Omega} \min_{y \in \partial D_a} \frac{|x - y|}{c} + T = t_2. \quad (25)$$

By superposition and repeating the above analysis for every $\omega = \omega_j$ in (11) we have that the field radiated by the time domain source density $q \in C(\partial D'_a, [0, T])$ given by

$$q(y, t) = \sum_{j=1}^N e^{-i\omega_j t} w_j(y) (H(t) - H(t - T)) \quad (26)$$

when $w_j \in C(\partial D'_a)$ is such that

$$\int_{\partial D'_a} \phi_{\omega_j}(x, y) w_j(y) dS_y \approx f_j(x) \text{ in } \Omega. \quad (27)$$

Here, the approximation is of order $\frac{\mu}{N}$ in $C^2(\Omega)$ where μ was the desired accuracy level introduced in (3). Hence,

$$\|v - \sum_{j=1}^N e^{-i\omega_j t} f_j\|_{(C[t_1, t_2], C^2(\Omega))} < \mu \quad (28)$$

This implies that the desired control effect (28) will not be felt in the time interval immediately after the opening of the sources, i.e., for $t \in \left(0, \max_{x \in \Omega} \max_{y \in \partial D_a} \frac{|x - y|}{c}\right)$. Then, the effect will be felt a bit after the sources shut down, i.e., in the time interval $\left(T, \min_{x \in \Omega} \min_{y \in \partial D_a} \frac{|x - y|}{c} + T\right)$. We can further implement delays and different stop times for each source so that we minimize the interval of incoherence and make the control effect smoother.

5.1.3 Time-domain Simulation

In what follows, we illustrate the above time-domain discussion in a simulation of the control problem inside a car cabin. We adopt the same geometrical configuration as in Section 5.1.1. We run a multitude of test in each of which we impose the planewave $f_q(\mathbf{x}) = e^{i\mathbf{x}\cdot(k_q(0,1,0))}$ on D_1 (the lower left control region in Figure 3) with $k_q = \overline{1, 50}$ and zero fields on the remaining three control regions, as well as the null sphere. The time-dynamic prescribed field f and generated field u are then obtained by superimposing the fields from the different frequencies scaled by the time dependent factor $e^{-ik_q ct}$, i.e.,

$$f(\mathbf{x}, t) = \sum_{q=1}^{50} f_q(\mathbf{x})e^{-ik_q ct} \text{ and } u(\mathbf{x}, t) = \sum_{q=1}^{50} u_q(\mathbf{x})e^{-ik_q ct}$$

where $c = 343$ m/s is the assumed speed of sound in the medium. We let $t \in [0, 0.04]$ so that the time-domain animations will show around two periods of the generated waves.

The results of the time-domain synthesis are shown in an animation found in [31]. The time-averaged plots of the prescribed and generated fields are shown in Figure 9. This shows a good visual match between the fields. The time-averaged relative error is around around 0.85 %. The plot of the pointwise relative errors is shown in Figure 10 while the time evolution of the pointwise relative error can be found in this animation [30].

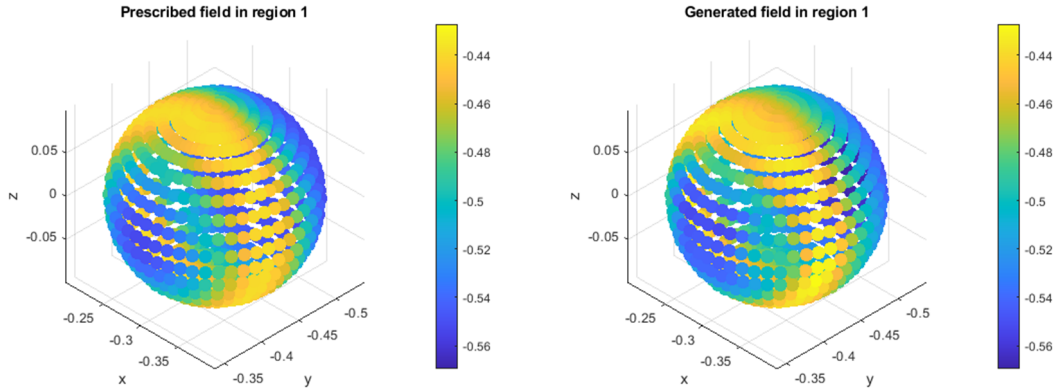


Figure 9: A visual comparison of the time-averaged real part of the prescribed and generated fields on D_1

The results on the other three near control regions are likewise good. The time-domain evolution is shown in the animation [28], while the time-averaged field values are shown in Figure 11. The figure shows that on the average, the field values are of order 10^{-3} , way below the magnitude of the field generated on D_1 .

Lastly, the field synthesized on the surface of the null sphere is also of small amplitude as seen in the time evolution animation found in [27] and in the time-averaged plot in Figure 12. The supremum of the time-averaged field is around 1.4×10^{-3} .

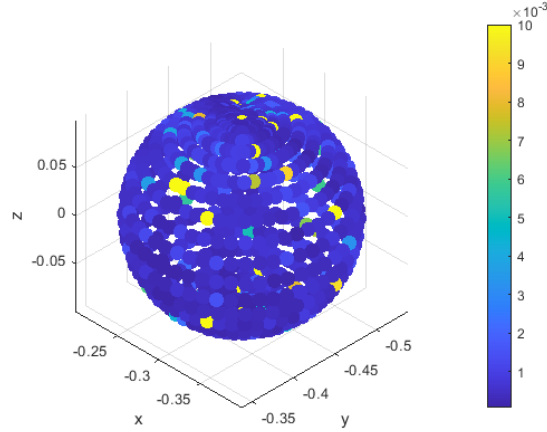


Figure 10: Plot of the time-averaged pointwise relative error

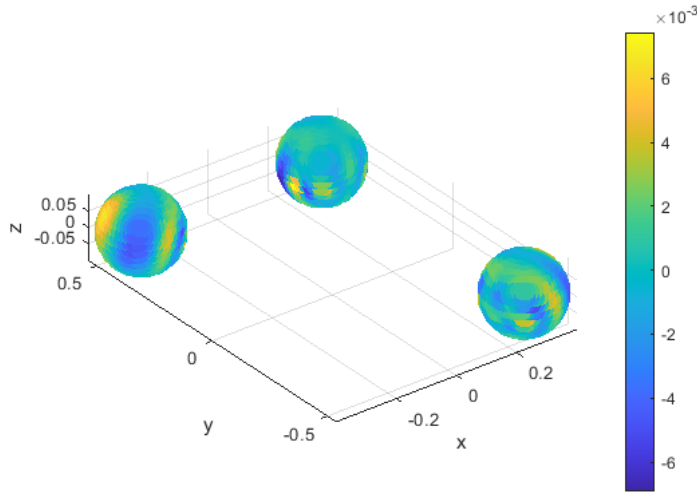


Figure 11: Plot of the time-averaged real part of the generated field on the remaining three control regions

We also mention here that in order to recreate personal sound experiences in each of the 4 control regions we can repeat the above procedure for each of the 4 regions and then superimpose the results to obtain the desired fast decaying field with controlled patterns in each of the four control regions. Also as observed in the analysis performed in Section 5.1.2 there will be an initial time interval $[0, t_1]$ with t_1 defined at (24), during which the desired control effect will not be observed. This interval is very small considering that the speed of sound is much larger than the distances considered in our problems and can further be minimized by introducing appropriate delays at each of the point sources in the overall array. This is why we believe that the effect of this short lived disturbance will be small

when interacting with the boundary of R .

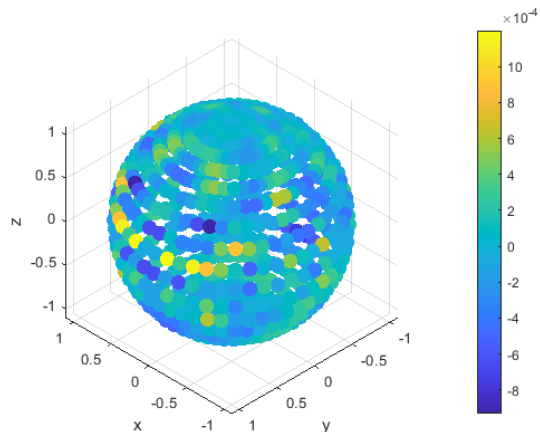


Figure 12: Plot of the time-averaged real part of the generated field in the surface of the null sphere

The time-averaged real part of the computed density and its corresponding normal velocity on each source are shown in Figure 13 and Figure 14 while the animated time-evolution can be found in [23] and [24], respectively. Even in the time domain, both the density and normal velocity exhibits a highly oscillatory and complex behavior.

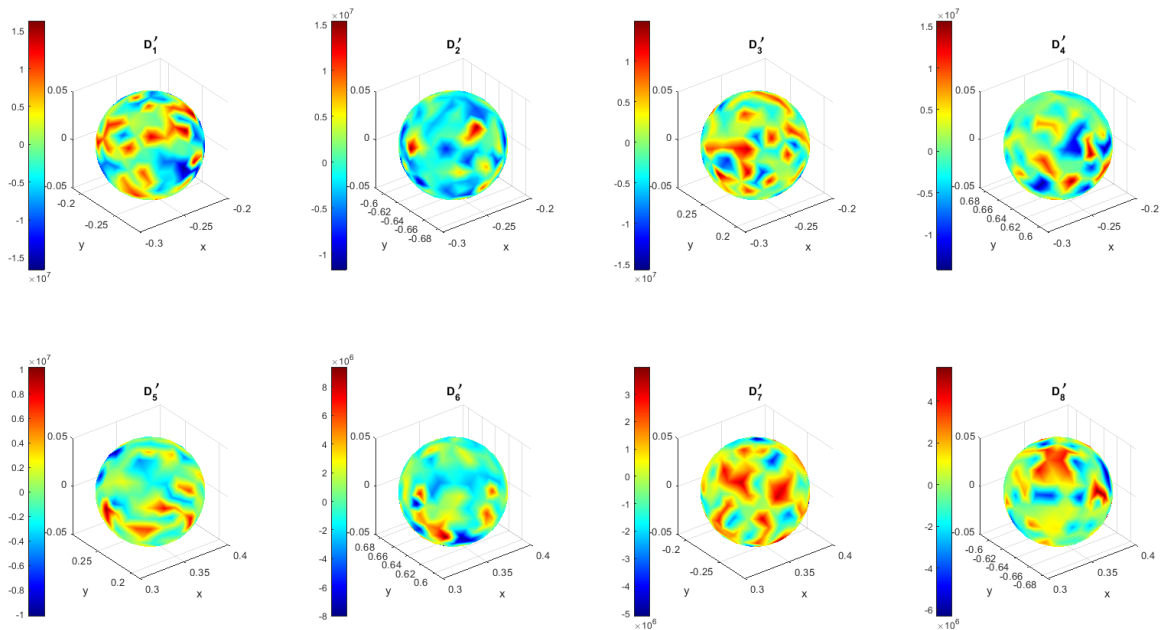


Figure 13: Time-averaged real part of the computed density on the fictitious sources

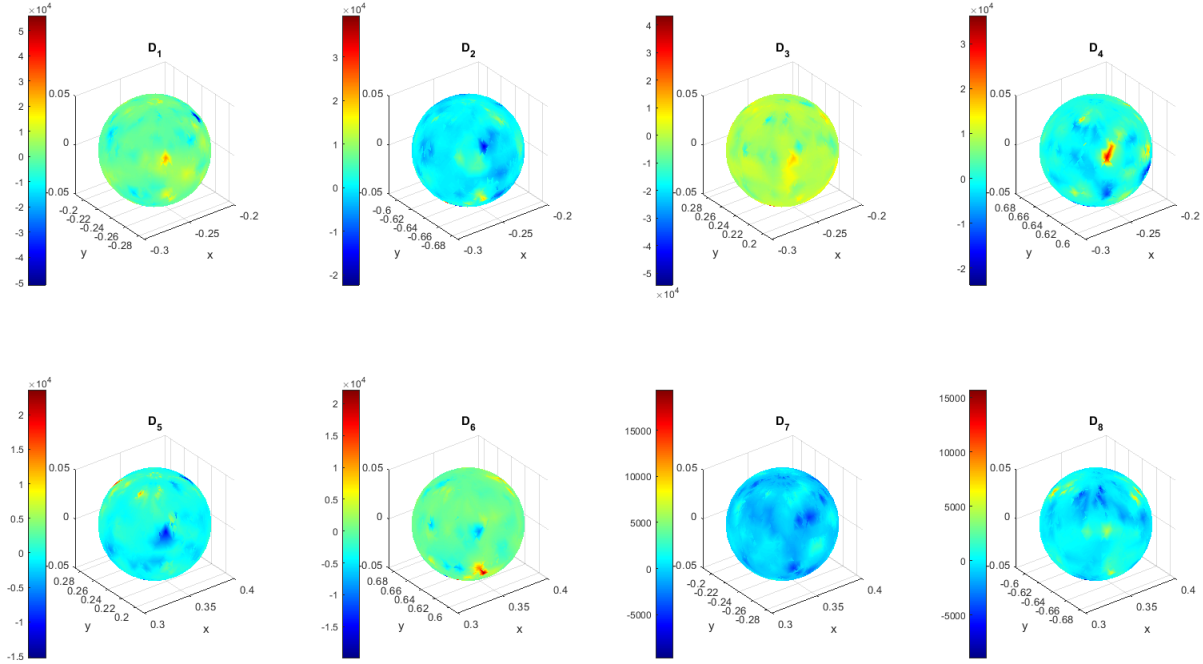


Figure 14: Time-averaged real part of the corresponding normal velocity on the physical sources

5.2 Shielded Localized Communications

In this simulation, we address the problem of creating shielded localized communication, i.e., establishing a desired sound profile in a given region exterior to the source array with very small field beyond a certain small radius, away from the array. We model the listening zone as a spherical control region of radius 25 cm with center at $(-0.52, 0, 0.20)$. Meanwhile, the source array is modeled by 12 spherical sources $D_i, i = \overline{1, 12}$ with radius 1 cm whose centers are uniformly distributed on the sides of a 7 cm by 15 cm rectangle (usual phone dimensions). The center of the rectangle is assumed to be at the origin, making its center 20 cm below the center of the control region. See Figure 2. The far control region, outside of which we want the acoustic field to be very small, is a sphere of radius 1.5 m concentric with the rectangle.

To demonstrate our scheme, we wish to create the plane wave $f(\mathbf{x}) = e^{i\mathbf{x} \cdot (k\hat{\mathbf{d}}_1)}$, where $\hat{\mathbf{d}}_1 = \langle 0, 1, 0 \rangle$ and wave number $k = 10$ (corresponding to about 546 Hz) on the near control while imposing a null field on the far control. Both control regions were discretized into 3200 collocation points.

The results of the field synthesis on the near control regions are shown in Figure 15. A visual comparison of these fields suggest a good match between the prescribed and generated fields. It is confirmed in Figure 16 where we see the pointwise relative errors. We see that throughout the near control, the relative error is just below 3%.

Meanwhile, the generated field on the surface of the null sphere is shown in Figure 17. It

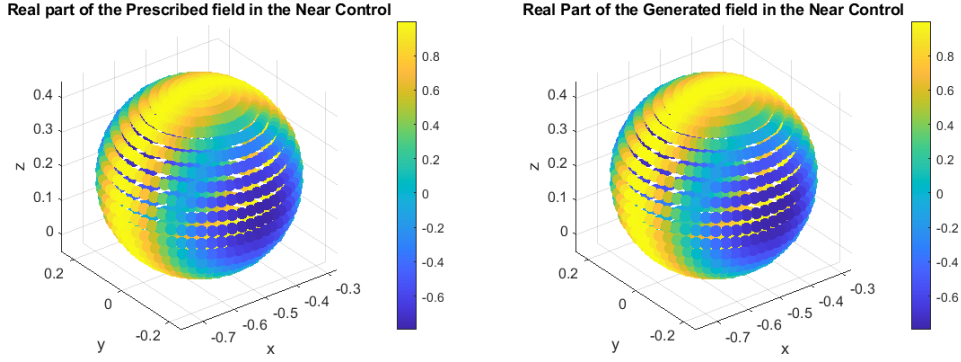


Figure 15: A visual comparison of the real part of the prescribed and generated fields on the control region

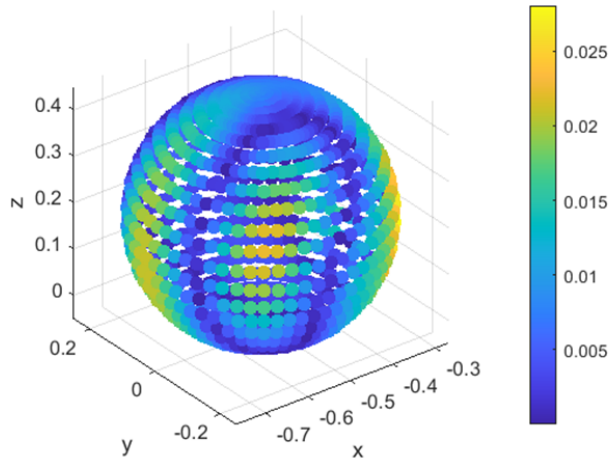


Figure 16: Plot of the pointwise relative error

can be noted that the generated field has supremum 8.29×10^{-3} , which is three orders lower than the field on the near control. This guarantees little spill over of the acoustic pressure that will ensure that observers beyond the far control will not receive an intelligible signal and obstacles beyond the sphere will not cause significant echo or reverberations.

Figure 18 and Figure 19 shows the generated field on the plane $z = 0$ and $z = 0.2$ respectively. The red circle is the projection of the far control on the planes while the black circles near the origin represent the projection of the boundary of the sources. The color maps on these plots are truncated to better show the variations in the magnitude of the field. These show that most of the radiated energy is focused on the area near the sources while decaying fast enough to achieve near zero magnitude on the far control region.

The computed density from the numerical scheme and the resulting normal velocity on each source are shown in Figure 20 and Figure 21, respectively. Both show complex patterns

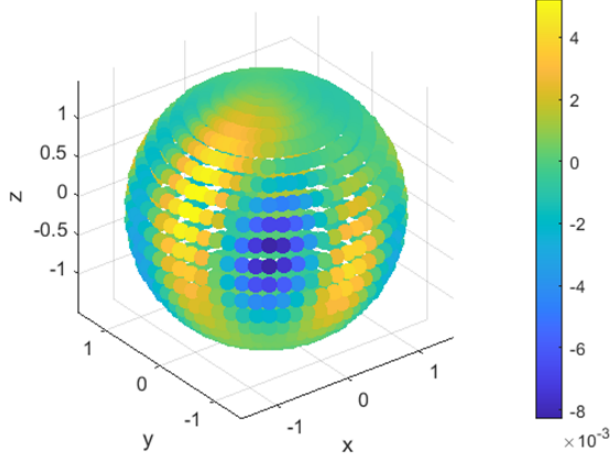


Figure 17: Plot of the real part of the generated field in the surface of the null sphere

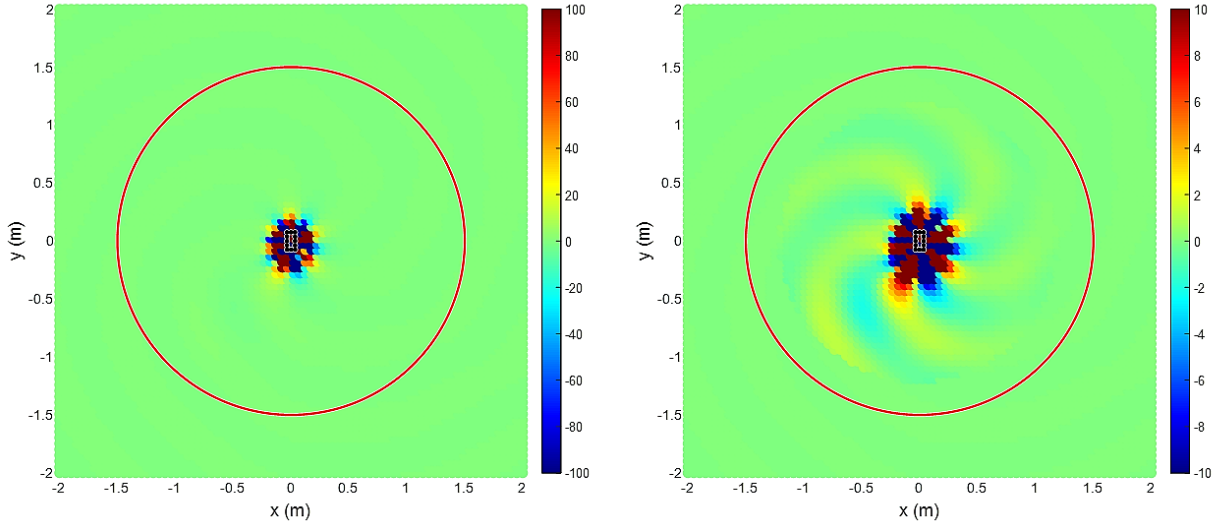


Figure 18: Real part of the generated field on the plane $z = 0$, the color map on the left plot is truncated to $[-100, 100]$ while the right plot's color bar is set to $[-10, 10]$ to show the radiated pattern in different scales

with oscillations that may be difficult for physical instantiation.

5.2.1 Time-domain Simulations: Shielded Localized Communications

Next we employ again the Fourier synthesis developed in the beginning of Section 5.1.2 to extend the above discussion to the time-domain. Thus, we run a multitude of tests in each of which we impose the planewave $f_q(\mathbf{x}) = e^{i\mathbf{x} \cdot (k_q \langle 0, 1, 0 \rangle)}$ on the near control with $k_q = \overline{1, 50}$ (corresponding to frequencies from around 54.59 Hz to 2.73 KHz) and a null field on the far control. The time-dynamic prescribed field f and generated field u are then obtained by

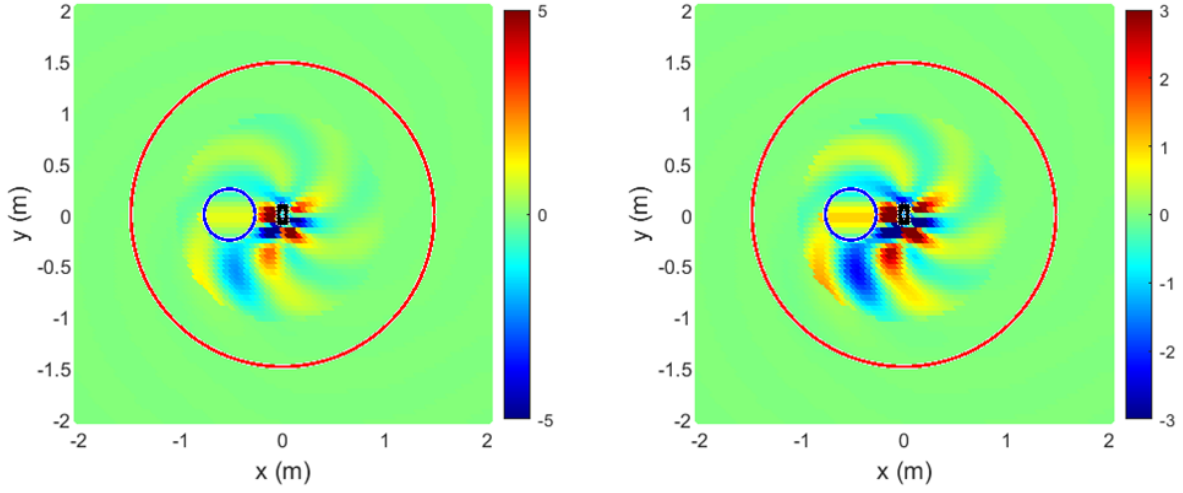


Figure 19: Real part of the generated field on the plane $z = 0.2$, the color map on the left plot is truncated to $[-5, 5]$ while the right plot's color bar is set to $[-3, 3]$ to show the radiated pattern in different scales

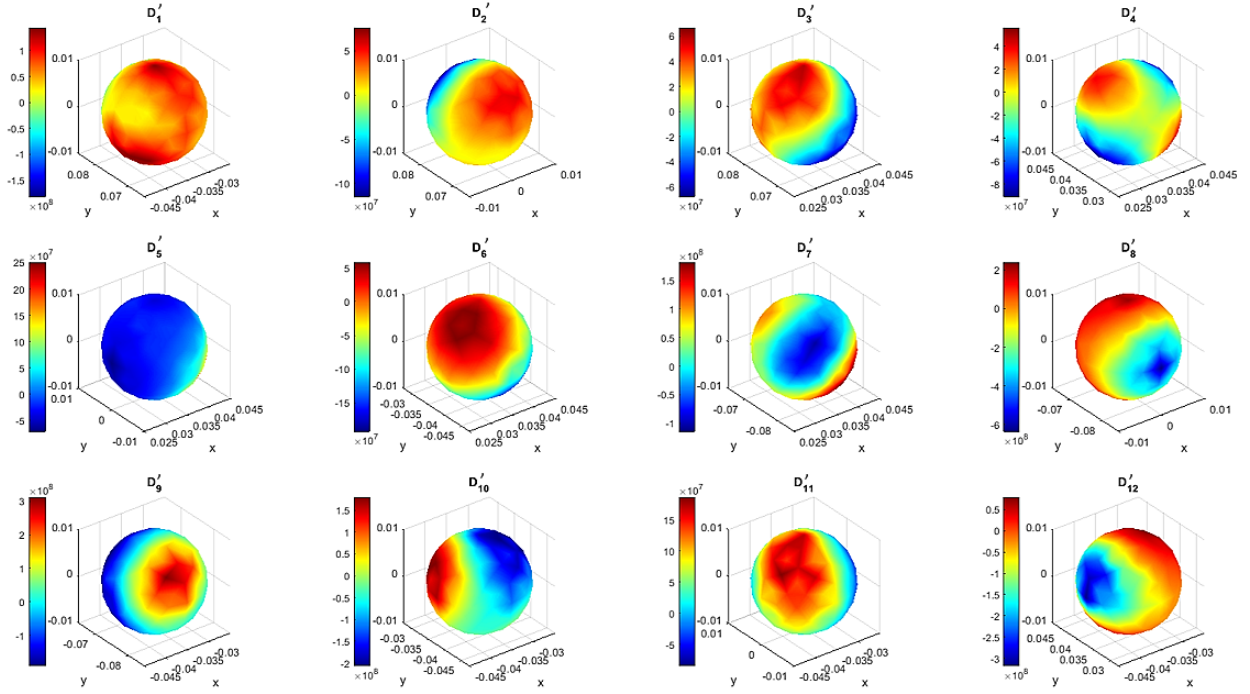


Figure 20: Real part of the computed density on the fictitious sources

superimposing the fields from the different frequencies scaled by the time dependent factor $e^{-ik_q ct}$, i.e.,

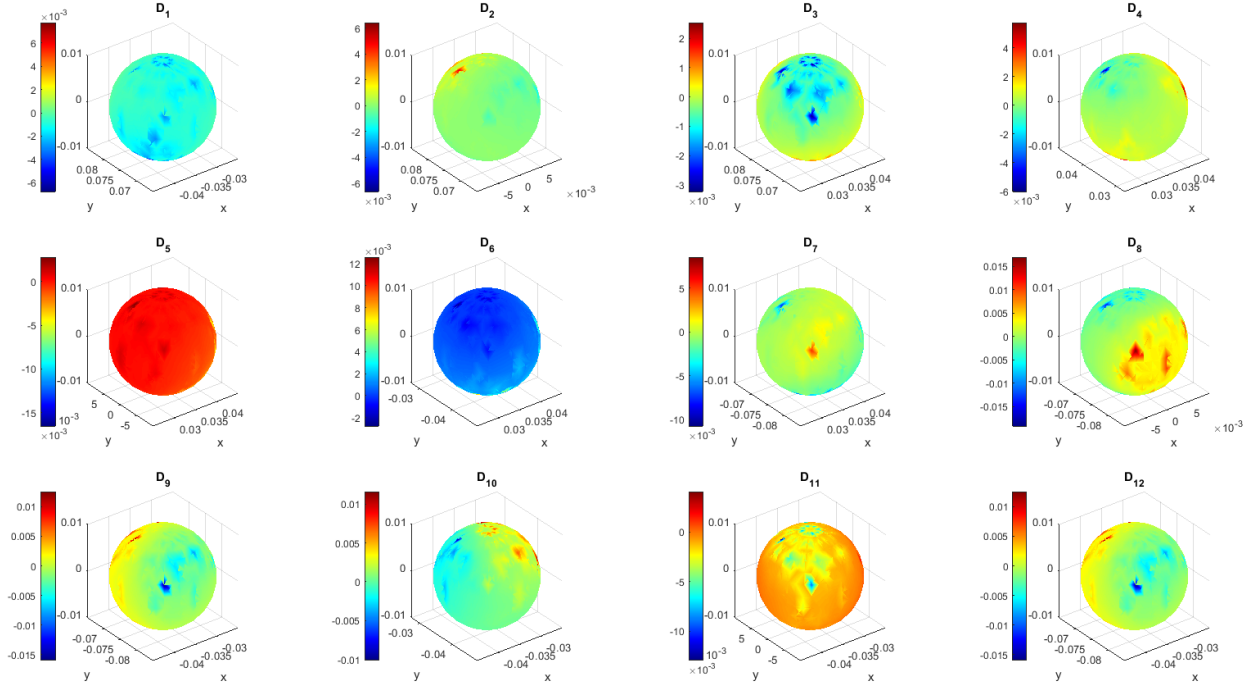


Figure 21: Real part of the corresponding normal velocity on the physical sources

$$f(\mathbf{x}, t) = \sum_{q=1}^{50} f_q(\mathbf{x})e^{-ik_q ct} \text{ and } u(\mathbf{x}, t) = \sum_{q=1}^{50} u_q(\mathbf{x})e^{-ik_q ct}$$

where $c = 343$ m/s is the assumed speed of sound in the medium. We let $t \in [0, 0.02]$ so that the time-domain animations will show around one period of the generated wave.

The results of the time-domain synthesis are shown in an animation found in [32]. The time-averaged plots of the prescribed and generated fields are shown in Figure 22. These show a good visual match between the fields. The time-averaged relative error is around around 3.87 %. The plot of the time-averaged pointwise relative errors is shown in Figure 23 while the time evolution of the pointwise relative error can be found in this animation [33]. In these plots, the color map was truncated to show the variations in the relative error better.

The field synthesized on the surface of the null sphere is also of small amplitude as seen in the time evolution animation found in [26] and in the time-averaged plot in Figure 24. The supremum of the time-averaged field is around 1.74×10^{-4} .

It is also of interest to observe the generated field on the cut plane $z = 0$ that cuts across the center of the sources. The complete time animation can be found in [29]. In this animation, the red circle shows the projection of the far control on $z = 0$, while the small black circles near the origin show the boundary of the sources. This show that the radiated energy is focused in the region near the sources and decays fast to achieve the near zero field

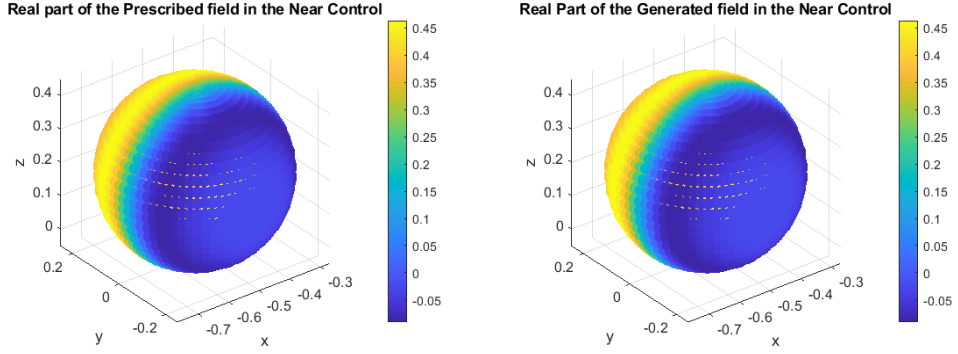


Figure 22: A visual comparison of the time-averaged real part of the prescribed and generated fields on the near control region

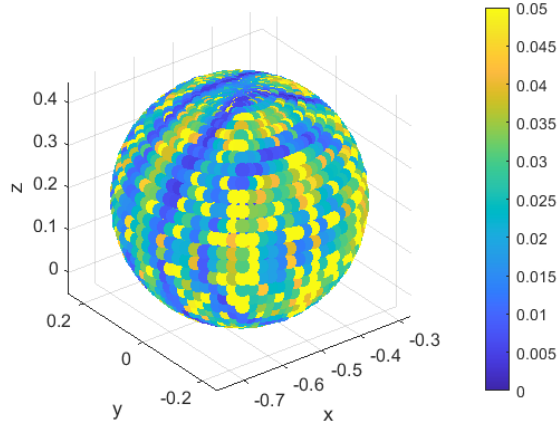


Figure 23: Plot of the time-averaged pointwise relative error

on the far control.

Lastly, Figure 25 shows time-averaged normal velocity, while its complete time evolution can be found in the animation in [25]. It can be noted that the complexity of the pattern and its oscillations in time may be challenging for physical instantiation.

6 Conclusion and future works

In this paper, we presented our strategy to achieve active control of acoustic fields in the context of two major applications: personal sound zones in bounded domains and shielded localized communications in free space. Our approach takes advantage of our previous works in the control of Helmholtz fields in free space using an almost non-radiating array of sources. We utilize the fact that we can design the desired source array by specifying a normal velocity (or surface pressure) on each source so that we can achieve desired fields in control regions

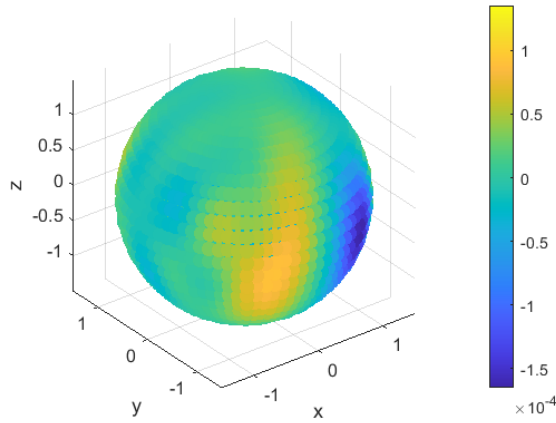


Figure 24: Plot of the time-averaged real part of the generated field in the surface of the null sphere

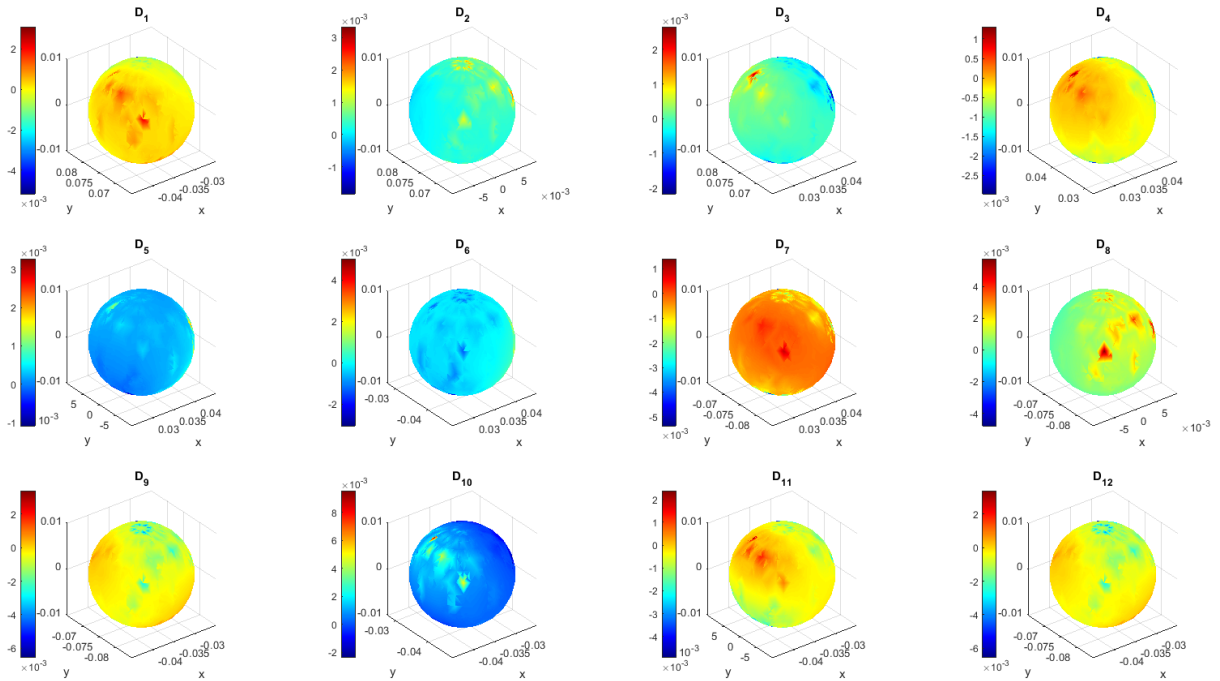


Figure 25: Plot of the time-averaged real part of the computed normal velocity

near the sources and a zero field in the surface of a null sphere that contains the control regions and is well-separated from the region's boundary. The non-radiating character of the array ensures the fast decay of the generated field. This is necessary so that the reverberations caused by the reflection of sound in the region's boundary will not significantly alter the primary field generated by the sources on the control region. This may overcome the need

to model the region’s boundary, which could possibly result to piecewise mixed boundary conditions for the Helmholtz equation.

The proposed approach was numerically implemented using a collocation method where the unknown density functions characterizing the normal velocities were represented using local basis functions. The resulting linear system was solved using Tikhonov regularization with the Morozov Discrepancy Principle to ensure the stability of the solution. Several numerical simulations were performed to illustrate the approach’s utility in practical applications. The simulation results showed a successful synthesis of the desired fields on the control regions while maintaining a field with small amplitude in the null sphere. We also mention here that the theoretical and numerical results suggest that our time-domain active control approach will work well for any band-limited signal.

One pressing challenge posed by the obtained results is the complexity of the source feed inputs. Recent advances in the sound synthesis literature suggest the possibility of using heat nanotubes and very small transducers to instantiate the computed normal velocities ([51, 61, 14, 10, 90]). Other possible approaches to remedy this difficulty would be the use of different norms, such as the L^1 and TV norms in the regularization process. These alternative regularization methods may temper the oscillations produced in the current setup using the L^2 norm.

Immediate extensions of this work include the performance of sensitivity tests with respect to variations in physically relevant problem parameters such as frequency, size of control regions, size and number of sources, distance between control regions and sources, relative position of control regions and sources, and the size of the null sphere and its distance from the region’s boundary. One may also venture in the application of the proposed method in controlling acoustic waves in other environments such as in a homogeneous ocean and in an ocean of two homogeneous layers. In these cases, one may take advantage of the theoretical, functional, and numerical schemes developed in the works [35, 37, 88, 36].

This work can also be extended to the control of electromagnetic waves in enclosed environments. Here, one can rely on the results established in [98, 79, 89, 87]. Specifically in [79], a scheme that uses the solution of the control problem of scalar Helmholtz fields to obtain smooth controls for the vectorial electromagnetic fields was developed utilizing Debye potentials.

Acknowledgment

NJA Egarguin’s work towards this paper was funded by the University of the Philippines System Enhanced Creative Work and Research Grant (ECWRG-2022-1-8R).

References

- [1] F. T. Agerkvist, P. Libianchi, and E. Shabalina. A review of techniques and challenges in outdoor sound field control. *Inter. Noise, Glasgow, 2022*.

- [2] Jens Ahrens. *Analytic Methods of Sound Field Synthesis*. T-Labs Series in Telecommunications Services. Springer, 2012.
- [3] Jens Ahrens. *Analytic Methods of Sound Field Synthesis*. Springer, 2012.
- [4] Jens Ahrens and Sascha Spors. Sound field reproduction using planar and linear arrays of loudspeakers. *IEEE Trans. Audio, Speech, Language Processing*, 18(8):2038–2050, 2010.
- [5] A. Albicker and R. Griesmaier. Monotonicity in inverse obstacle scattering on unbounded domains. *Inverse Problems*, 36, 2020.
- [6] A. Albicker and R. Griesmaier. Monotonicity in inverse scattering for Maxwell’s equations. *Inverse Problems and Imaging*, 2022.
- [7] Thomas S. Angell and Andreas Kirsch. *Optimization Methods in Electromagnetic Radiation*. Springer Monographs in Mathematics. Springer-Verlag New York, 2004.
- [8] Albicker Annalena. *Monotonicity methods for inverse scattering problems*. Dissertation at the Institut für Angewandte und Numerische Mathematik (IANM), 2023.
- [9] Tilo Arens, Roland Griesmaier, and Ruming Zhang. Monotonicity-based shape reconstruction for an inverse scattering problem in a waveguide. *Inverse Problems*, 39(7), 2023.
- [10] S. S. Asadzadeh, A. Moosavi, C. Huynh, and O. Saleki. Thermo acoustic study of carbon nanotubes in near and far field: Theory, simulation, and experiment. *Journal of Applied Physics*, 117:095101, 2015.
- [11] Lander Besabe and Daniel Onofrei. Active control of scalar helmholtz fields in the presence of known impenetrable obstacles. *AMS Contemporary Mathematics*, 2022.
- [12] Yuri Bobrovnikskii. Impedance acoustic cloaking. *New J. Phys*, 12:043049, 2010.
- [13] Charles Allan Boyles. *Acoustic Waveguides: Applications to Oceanic Science*. Wiley-Interscience, New York, 1984.
- [14] J. J. Brown, N. C. Moore, J. C. Gertsch O. D. Supekar, and V. M. Bright. Ultrathin thermoacoustic nanobridge loudspeakers from ALD on polyimide. *Nanotechnology*, 27(47):475504, 2016.
- [15] James L. Buchanan, Robert P. Gilbert, Armand Wirgin, and Yongzhi S. Xu. *Marine Acoustics: Direct and Inverse Problems*. SIAM, 2004.
- [16] Jordan Cheer. Active control of scattered acoustic fields: cancellation, reproduction and cloaking. *J. Acoust. Soc. Am.*, 140(3):1502–1512, 2016.

- [17] Jordan Cheer and Stephen J. Elliott. Multichannel control systems for the attenuation of interior road noise in vehicles. *Mech. Syst. Signal Process.*, 60-61:753–769, 2015.
- [18] David Colton and Rainer Kress. *Integral Equation Methods in Scattering Theory*. Classics in Applied Mathematics 72. SIAM, Philadelphia, 2013.
- [19] P. Couturier, P.A. Nelson, T. Takeuchi, and X. Zhou. Sound field control for multiple listener virtual imaging. *Journal of Sound and Vibration*, 539, 2022.
- [20] R. C. de Lamare, Z. Zheng, Y. Yu, X. Yang, L. Lu, K.i-L. Yin, and B. Chen. A survey on active noise control in the past decade - part i: Linear systems. *Signal Processing*, 183, 2021.
- [21] R. C. de Lamare, Z. Zheng, Y. Yu, X. Yang, L. Lu, K.i-L. Yin, and B. Chen. A survey on active noise control in the past decade - part ii: Nonlinear systems. *Signal Processing*, 181, 2021.
- [22] Anthony J. Devaney. *Mathematical Foundations of Imaging, Tomography and Wave-field Inversion*. Cambridge University Press, 2012.
- [23] Neil Jerome A. Egarguin. Animation of the calculated density. https://drive.google.com/file/d/156-7petf-WnL5XTtgfdo_10Hkp0eBPC9/view?usp=sharing, Generated: April 2024.
- [24] Neil Jerome A. Egarguin. Animation of the calculated normal velocity. https://drive.google.com/file/d/1tu0N8kceMN-MXc1FWrptUkB4hu1ccrC_/view?usp=drive_link, Generated: April 2024.
- [25] Neil Jerome A. Egarguin. Animation of the computed normal velocity for the phone simulation. https://drive.google.com/file/d/1muIxzdtH9dHxDmaz85A0CIf4QtmWLOr0/view?usp=drive_link, Generated: October 2024.
- [26] Neil Jerome A. Egarguin. Animation of the generated field on the far control region for the phone simulation. https://drive.google.com/file/d/16N10wdksIkev5CIGFqqNzsoUbWUEqo70/view?usp=drive_link, Generated: October 2024.
- [27] Neil Jerome A. Egarguin. Animation of the generated field on the null sphere. <https://drive.google.com/file/d/1hjrLn9E3AwteooUh-4ITelMYmuEYt8ps/view?usp=sharing>, Generated: April 2024.
- [28] Neil Jerome A. Egarguin. Animation of the generated field on the other three near control regions. <https://drive.google.com/file/d/15CqM5PgcNbrRB6U42nwTl50mX-k1bY9T/view?usp=sharing>, Generated: April 2024.

- [29] Neil Jerome A. Egarguin. Animation of the generated field on the plane $z = 0$. https://drive.google.com/file/d/1SMs3jb575L83aQ1R2HFjOWu4VycF33Hv/view?usp=drive_link, Generated: October 2024.
- [30] Neil Jerome A. Egarguin. Animation of the pointwise relative error. <https://drive.google.com/file/d/1YN0Buup-A-DEDit7s6KpR9Bx-y6kwBwB/view?usp=sharing>, Generated: April 2024.
- [31] Neil Jerome A. Egarguin. Animation of the prescribed and generated fields on the near control d_1 . <https://drive.google.com/file/d/126kmb0eP2xc905jTqkCZUcm2CY5AKRg/view?usp=sharing>, Generated: April 2024.
- [32] Neil Jerome A. Egarguin. Animation of the prescribed and generated fields on the near control region for the phone simulation. https://drive.google.com/file/d/1Q0zImcZr2cWgWU3TP9xGotXCLi_rou0a/view?usp=drive_link, Generated: October 2024.
- [33] Neil Jerome A. Egarguin. Animation of the relative errors in the near control region for the phone simulation. https://drive.google.com/file/d/1ooW1VWyUbhfbQ_8VIJSMgKCltMuZ5PER/view?usp=drive_link, Generated: October 2024.
- [34] Neil Jerome A. Egarguin, Daniel Onofrei, and Eric Platt. Sensitivity analysis for the active manipulation of Helmholtz fields in 3d. *Inverse Probl. Sci. Eng.*, 28(3):314–339, 2020.
- [35] Neil Jerome A. Egarguin, Daniel Onofrei, Chaoxian Qi, and Jiefu Chen. Active manipulation of Helmholtz scalar fields: Near-field synthesis with directional far-field control. *Inverse Probl.*, 36(9), 2020.
- [36] Neil Jerome A. Egarguin, Daniel Onofrei, Chaoxian Qi, and Jiefu Chen. Active manipulation of helmholtz scalar fields in an ocean of two homogeneous layers of constant depth. *Inverse problems in Science and Engineering*, 29(13):2491–2515, 2021.
- [37] Neil Jerome A. Egarguin, Shubin Zeng, Daniel Onofrei, and Jiefu Chen. Active control of Helmholtz fields in 3d using an array of sources. *Wave Motion*, 94(102523):1–27, 2020.
- [38] Daniel Egglera, Hyuck Chung, Fabien Montiel, Jie Pan, and Nicole Kessissoglou. Active noise cloaking of 2d cylindrical shells. *Wave Motion*, 87:106–112, 2019.
- [39] Stephen Elliot. *Signal Processing for Active Control*. Academic Press, 1st edition, 2001.
- [40] Stephen J. Elliot, Jordan Cheer, Jung-Woo Choi, and Youngtae Kim. Robustness and regularization of personal audio systems. *IEEE Trans. Audio, Speech, Language process.*, 20(7):2123–2133, 2012.

- [41] Chris R. Fuller and Andreas H. von Flotow. Active control of sound and vibration. *IEEE Control Systems Magazine*, 15(6):9–19, Dec 1995.
- [42] Wilfried Gallian, Filippo Maria Fazi, Carlo Tripodi, Nicolo Strozzi, and Alessandro Costalunga. Optimisation of the target sound fields for the generation of independent listening zones in a reverberant environment. *IEEE Explore*, 2021 Immersive and 3D Audio: from Architecture to Automotive(I3DA), 2021.
- [43] Hao Gao, Jiazheng Cheng, Ziyun Liu, and Yong Shen. Multizone sound reproduction with adaptive control of scattering effects. *J. Acoust. Soc. Am.*, 153:835– 847, 2023.
- [44] J. Garcia-Bonito and S.J. Elliott. Active cancellation of acoustic pressure and particle velocity in the near field of a source. *J. Sound Vib.*, 221(1):85 – 116, 1999.
- [45] R. Griesmaier and B. Harrach. Monotonicity in inverse medium scattering on unbounded domains. *SIAM Journal of Appl. Math.*, 78(5), 2018.
- [46] R. Griesmaier and B. Harrach. Erratum: Monotonicity in inverse medium scattering on unbounded domains. *SIAM Journal of Appl. Math.*, 81(3):1332– 1337, 2021.
- [47] Dieter Guicking. *Active control of sound and vibration history - fundamentals - state of the art*. Festschrift DPI, Universitätsverlag Gottingen, 2007.
- [48] Zerui Han, Ming Wu, Qiaoxi Zhu, and Jun Yang. Two-dimensional multizone sound field reproduction using a wave-domain method. *J. Acoust. Soc. Am.*, 144, 2018.
- [49] Zerui Han, Ming Wu, Qiaoxi Zhu, and Jun Yang. Three-dimensional wave-domain acoustic contrast control using a circular loudspeaker array. *J. Acoust. Soc. Am.*, 145, 2019.
- [50] Charlie House, Jordan Cheer, and Steve Daley. On the use of virtual sensing for the real-time detection and active control of a scattered acoustic field. *International Congress of Sound and Vibration*, 2019.
- [51] Hanping Hu, Dongdong Wang, and Zedong Wang. Solution for acoustic field of thermo-acoustic emission from arbitrary source. *AIP Advances*, 4(10):107114, 2014.
- [52] N. Hu and S.V. Utyuzhnikov. Optimized nonlocal active sound control in frequency domain. *Applied Acoustics*, 187, 2022.
- [53] Mark Hubenthal and Daniel Onofrei. Sensitivity analysis for active control of the Helmholtz equation. *Appl. Numer. Math.*, 106:1–23, 2016.
- [54] M. Ikehata. An approach based on the wave equation in the time domain for active shielding of an unwanted wave with a fixed frequency. *arxiv.org*, arXiv:2107.09849, 2021.

- [55] F.B. Jensen, W.A. Kuperman, M.B. Porter, and H. Schmidt. *Computational Ocean Acoustics*. Springer, New York, 2011.
- [56] Wenyu Jin, W. Bastiaan Kleijn, and David Virette. Multizone soundfield reproduction using orthogonal basis expansion. *2013 IEEE International Conference on Acoustics, Speech and Signal Processing*, pages 311–315, 2013.
- [57] Joseph B. Keller and John S. Papadakis. *Wave Propagation and Underwater Acoustics*. Number 70 in Lecture Notes in Physics. Springer-Verlag, Berlin, Heidelberg, 1977.
- [58] Sang-Myeong Kim, Joao A. Pereira, Antonio E. Turra, and Jun-Ho Cho. Modeling and dynamic analysis of an electrical Helmholtz resonator for active control of resonant noise. *J. Vib. Acoust.*, 139(5), 2017.
- [59] Taewoong Lee. *The creation of perceptually optimized sound zones using variable span trade-off filters*. Dissertation at the Aalborg University, Denmark, 2021.
- [60] P. Leug. *Process of Silencing Sound Oscillations*. U.S. Patent No.2043416. 1936.
- [61] C.W. Lim, L.H. Tong, and Y.C. Li. Theory of suspended carbon nanotube thinfilm as a thermal-acoustic source. *Journal of Sound and Vibration*, 332(21):5451–5461, 2013.
- [62] Jingwei Liu, Xiaolin Wang, Ming Wu, and Jun Yang. An active control strategy for the scattered sound field control of a rigid sphere. *J. Acoust. Soc. Am.*, 144(EL52), 2018.
- [63] J. Lončarić, V. S. Ryaben’kii, and S. V. Tsynkov. Active shielding and control of noise. *SIAM J. Appl. Math.*, 62(2):563–596, 2001.
- [64] J. Lončarić and S. V. Tsynkov. Optimization of acoustic source strength in the problem of active noise control. *SIAM J. Appl. Math.*, 63(4):1141– 1183, 2003.
- [65] J. Lončarić and S. V. Tsynkov. Optimization of power in the problems of active control of sound. *Math. and Computers in Simulation*, 65:323 – 335, 2004.
- [66] J. Lončarić and S. V. Tsynkov. Quadratic optimization in the problems of active control of sound. *Appl. Numer. Math.*, 52:381–400, 2005.
- [67] Rajabi Majid and Mojahed Alireza. Active acoustic cloaking spherical shells. *Acta Acust. United with Ac.*, 104(1):5–12, 2019.
- [68] Qibo Mao, Shengquan Li, and Weiwei Liu. Development of a sweeping Helmholtz resonator for noise control. *Appl. Acoust.*, 141:348 – 354, 2018.
- [69] P. A. Martin. *Multiple Scattering Interaction of Time-Harmonic Waves with N Obstacles*. Cambridge University Press, 1st edition, 2006.

- [70] Dylan Menzies. Sound field synthesis with distributed modal constraints. *Acta Acust. Acust.*, 98(1):15–27, 2012.
- [71] D. A. B Miller. On perfect cloaking. *Opt. Express*, 14:12457–12466, 2006.
- [72] P. A. Nelson and S. J. Elliott. *Active Control of Sound*. Academic London, 1992.
- [73] P.A. Nelson and S.J. Elliot. The active control of sound. *Electronics and Comm. Engineering Journal*, 1990.
- [74] H.F. Olson and E.G. May. Electronic sound absorber. *J. Acad. Soc. Am.*, 25:1130–1136, 1953.
- [75] Akira Omoto, Shiro Ise, Yusuke Ikeda, Kanako Ueno, Seigo Enomoto, and Maori Kobayashi. Sound field reproduction and sharing system based on the boundary surface control principle. *Acoust. Sci. Technol.*, 36:1–11, 01 2015.
- [76] Daniel Onofrei. On the active manipulation of fields and applications. i - the quasistatic regime. *Inverse Probl.*, 28(10):105009, 2012.
- [77] Daniel Onofrei. Active manipulation of fields modeled by the Helmholtz equation. *J. Integral Equations Appl.*, 26(4):553–579, 2014.
- [78] Daniel Onofrei and Eric Platt. On the synthesis of acoustic sources with controllable near fields. *Wave Motion*, 77:12–27, 2018.
- [79] Daniel Onofrei, Eric Platt, and Neil Jerome A. Egarguin. Active manipulation of exterior electromagnetic fields by using surface sources. *Quarterly of Appl. Math.*, 78:641–670, 2020.
- [80] N. Peake and D. G. Crighton. Active control of sound. *Annu. Rev. Fluid Mech.*, 32:137–164, 2000.
- [81] A.W. Peterson and S.V. Tsynkov. Active control of sound for composite regions. *SIAM J. Appl. Math.*, 67(6):1582– 1609, 2007.
- [82] Roy Pike and Pierre Sabatier. *Scattering and inverse scattering in pure and applied science*. Academic Press, 1st edition, 2002.
- [83] V. Pohjola, B. Harrach, and M. Salo. Monotonicity and local uniqueness for the Helmholtz equation. *Analysis and PDE*, 12(7):1741– 1771, 2019.
- [84] Anastasis C. Polycarpou. *Introduction to the Finite Element Method in Electromagnetics*. Synthesis Lectures on Computational Electromagnetics. Morgan & Claypool Publishers, 2006.
- [85] B.I. Popa, D. Shinde, A. Konneker, and S. A. Cummer. Active acoustic metamaterials reconfigurable in real time. *Phys. Rev. B*, 91, 2015.

- [86] Chaoxian Qi, Neil Jerome A. Egarguin, Daniel Onofrei, and Jiefu Chen. Feasibility analysis for active near field/far field acoustic pattern synthesis in free space and shallow water environments. *Acta Acustica*, 5(39), 2021.
- [87] Chaoxian Qi, Neil Jerome A. Egarguin, Shubin Zeng, Daniel Onofrei, and Jiefu Chen. Sensitivity analysis for active electromagnetic field manipulation in free space. *Applied Mathematics in Science and Engineering*, 30(1):661–687, 2022.
- [88] Chaoxian Qi, Chenpei Huang, Neil Jerome Egarguin, Daniel Onofrei, Miao Pan, and Jiefu Chen. Enhanced underwater acoustic communication via active field control. In *WUWNet '21: Proceedings of the 15th International Conference on Underwater Networks and Systems*, 2022.
- [89] Chaoxian Qi, Shubin Zeng, Neil Jerome A. Egarguin, Daniel Onofrei, and Jiefu Chen. Active control of electromagnetic fields in layered media. *Journal of Electromagnetic Waves and Applications*, 38(1):66–88, 2023.
- [90] Yancong Qiao, Guangyang Gou, Fan Wu, Jinming Jian, Xiaoshi Li, Thomas Hirtz, Yunfei Zhao, Yao Zhi, Fangwei Wang, He Tian, Yi Yang, and Tian-Ling Ren. Graphene-based thermoacoustic sound source. *ACS Nano*, 14(4):3779–3804, 2020. PMID: 32186849.
- [91] Galvez Marcos F. Simon, Menzies Dylan, and Fazi Filippo Maria. Dynamic audio reproduction with linear loudspeaker arrays. *J. Asian Earth Sci.*, 67(4):190–200, 2019.
- [92] Fernando Guevara Vasquez, Graeme W. Milton, and Daniel Onofrei. Active exterior cloaking. *Phys. Rev. Lett.*, 103:073901, 2009.
- [93] Fernando Guevara Vasquez, Graeme W. Milton, and Daniel Onofrei. Broadband exterior cloaking. *Opt. Express*, 17(17):14800–14805, 2009.
- [94] Fernando Guevara Vasquez, Graeme W. Milton, and Daniel Onofrei. Exterior cloaking with active sources in two dimensional acoustics. *Wave Motion*, 48:515–524, 2011.
- [95] M. Wu, J. Yang, and L. Han. A review of sound field control. *Applied Sciences*, 12(14), 2022.
- [96] Li Xun, Van Manen Dirk-Jan, Robertsson Johan O.A., and Curtis Andrew. Soundscape immersion using imperfect sources. *ETH Research Collection submitted to Physical Review X*, 2019.
- [97] Cheuk-Him Yeung. *Active Noise Control: Lecture Notes in Physics*. Department of Mathematics, University of Manchester, 2022.
- [98] Shubin Zeng, Neil Jerome Egarguin, Daniel Onofrei, and Jiefu Chen. Active control of electromagnetic waves in layered media using a current source. In *2020 IEEE Texas Symposium on Wireless and Microwave Circuits and Systems*, 2020.

- [99] Junqing Zhang, Wen Zhang, Thushara D. Abhayapala, Jingli Xie, and Lijun Zhang. 2.5d multizone reproduction with active control of scattered sound fields. *IEEE Explore*, 2019 IEEE International Conference on Acoustics, Speech and Signal Processing, 2019.
- [100] Wen Zhang, Thushara D. Abhayapala, Terence Betlehem, and Filippo Maria Fazi. Analysis and control of multi-zone sound field reproduction using modal-domain approach. *J. Acoust. Soc. Am.*, 140(3):2134–2144, 2016.